

Equivalent Dielectric property of hydrogenated carbon nitride film in CH₄/N₂ DBD plasma: Gas and Solid phase reaction

Abhijit Majumdar,^{1,3,†} Sandhan Chandra Das,¹ Basudev Ghosh², Rainer Hippler¹

¹Institute of Physics, University of Greifswald, Felix Hausdorff Strasse 6, 17489 -Greifswald, Germany

²Department of Physics, Jadavpur University, Kolkata 700032, West Bengal, India

³Indian Institute of Engineering Science and Technology, Shibpur, Howrah-3, West Bengal, India

[†]Corresponding author: Abhijit Majumdar, email: majuabhijit@gmail.com

ABSTRACT : We report the equivalent dielectric property and chemical bond structure of hydrogenated carbon nitride (a-H-C_xN_y) film deposited in CH₄/N₂ (1:2) dielectric barrier discharge (DBD) plasma. Mass spectrum of CH₄/N₂ DBD plasma shows the several higher order hydrocarbons (a-H-C_xN_y, with x is up to 9), different functional CN groups produced in gas phase. Several N-1s, C-1s and O-1s peaks have been identified by x-ray photoelectron spectroscopy (XPS) and it shows that the formation of C–C, C=C, and C–H bond in the film is invariant with deposition time. Fourier transformed infrared spectroscopy (FTIR) spectra depict the presence of different functional including NH-OH, C≡N, CH₂, CH₃, C–N groups in the deposited film. Round shaped island growth has been observed at film surface area in scanning electron microscopy (SEM). Moreover, we proposed a crude assumption to estimate the equivalent dielectric constant of the film during the deposition process. The dielectric constant of a-H-C_xN_y film is measured (ex situ) by impedance analyzer and compared with the same obtained by Lissajous figure. The probable physical causes and importance of the results obtained are also pointed out.

KEYWORDS: Plasma deposition, hydrogenated carbon nitride film, Dielectric properties, Photoelectron spectroscopy, Infrared spectroscopy.

I. INTRODUCTION

Plasma assisted thin film deposition is currently the most promising field of deposition techniques [1-4]. It is an important and growing field in plasma technology. In order to improve the film depositions (i.e. deposition rate, film quality, film uniformity) numerical modeling of the plasma discharge can be of much use in achieving a better understanding of the various factors involved in the film deposition process. The properties of the deposited film are influenced by the plasma characteristics and the specific deposition conditions such as power, gas mixture and gas flow. Some models [5-10] have been developed for lower moderate pressure systems and for thermal plasmas where the reaction mechanisms are governed by the neutral gas temperature. In plasma deposition, the growth of low-molecular-weight molecules into high-molecular-weight molecules (polymers) occurs with the assistance of the plasma energy, which involves energetic electrons, ions, and radicals [11-12]. Plasma polymerization is a thin film forming process, where thin films are deposited directly on surfaces of the substrate without any fabrication. Advantages of the DBD for the wide field of applications are the non-thermal plasma conditions at low gas temperatures and at elevated (typically atmospheric) pressure. Dielectric barrier discharge (DBD) plasma offers attractive perspectives for the polymer coating deposition and surface functionalization as it provides easily applicable systems in industrial process [13-18]. Our present interest is on a-HCN_x film which has significant contributions to the tribological properties, chemical inertia, optical properties, bio-sensor [19], IR detectors [20], sterilization [21-24], ultra low dielectric property [17] and biomedical applications [24-28]. a-HCN_x film is deposited by atmospheric pressure dielectric barrier discharge plasma in mixture of CH₄/N₂ gases. In our previous study, a-HCN_x film deposited by CH₄/N₂ DBD plasma offers low dielectric property [17]. The materials having low dielectric property are promising candidate in semiconductor processing technology with a view to improve device performance.

During CH₄/N₂ plasma deposition we observed that the dielectric properties of the depositing film changes with time. Moreover, the dielectric properties of a-HCN_x layer when taken out after the deposition process are different from that observed during the plasma deposition process. In our previous work we proposed a linear model that correlates the surface temperature and surface polarization with thin film properties during the deposition process [12]. The change in temperature at the electrode surface was shown to depend on

the value of polarization and the in-situ dielectric constant of the deposited layer. The purpose of the work at 300 mbar pressure is to avoid uneven short circuit during the discharge process.

We have cross checked and compare the results obtained by atmospheric pressure and 300 mbar pressure DBD discharge and they are almost similar except some variation in the intensity (the results is not shown here). In this paper, we report the chemical bond structure of hydrogenated carbon nitride (a-H-C_xN_y) film and its associated gas phase reaction/product taking place during CH₄/N₂ DBD plasma process. Another aspect is that we propose a crude model to estimate the equivalent dielectric constant of a-H-C_xN_y film during the deposition process. We would like to mention that the gas phase reaction part is the extension of our previous work and few results (fig 5 and 9) are partly borrowed from our previous work [12, 18] for the comparative study. We report the chemical bonding structure of hydrogenated carbon nitride (a-HCN_x) film and its gas phase reaction mechanism in CH₄/N₂ (1:2) dielectric barrier discharge (DBD) plasma.

II. EXPERIMENTAL METHOD

A. Experimental set up

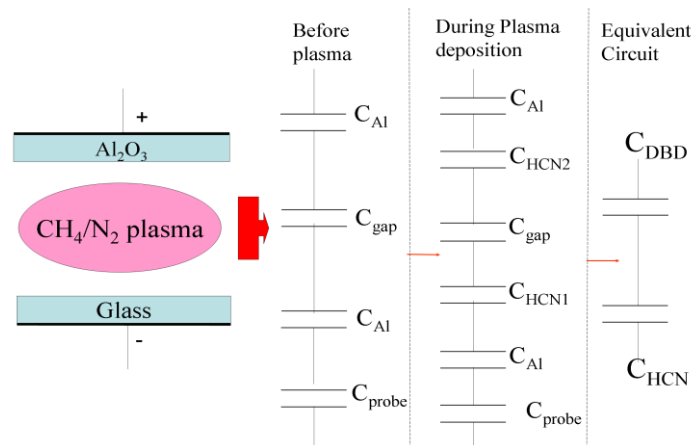


Figure 2. Variation of thickness of the deposited a-HCN_x film as a function of deposition time (minutes).

Figure 1 shows the equivalent capacitance circuit configuration of our DBD system which is similar to that used in ref [29]. The plasma chamber is made of stainless steel. The inner dimensions of the chamber are height 12.3 cm, length 18.0 cm, and width 15.0 cm, yielding a chamber volume of 3.32 dm³. The two electrodes are made from Cu plates with a length of 8.3 cm, width 3.3 cm, and thickness 0.15 cm. Both Cu electrodes are covered by aluminum oxide ($\epsilon \approx 10$). Both electrodes are separated by 0.20 cm from each other. The upper electrode is connected to a home-built high voltage power supply, while the lower electrode is grounded. The chamber is pumped by a membrane pump down to about 10 mbar. Pressure inside the plasma chamber was controlled by two gas flow controllers (MKS) for methane and nitrogen and by an adjustable needle valve between the chamber and the membrane pump. The experiments were performed with the chamber filled at a pressure of 300 mbar and with pump and gas flow shut off. The high voltage power supply consists of a frequency generator delivering a sinusoidal output that is fed into an audio amplifier. The amplifier can be operated at up to 500 W; its output is fed into a spark plug transformer. Experiments were performed at 12 kV (peak-to-peak) and at 6 kHz. The electrical power under these conditions was 5 W. It was measured by placing a probe capacitor (10 nF) between the lower electrode and ground and measuring the collected charge together with the applied voltage as function of time, as described by Wagner and Sonnenfeld et al. [30, 31].

B. Film characterization : X-ray photoelectron spectroscopy (XPS) measurements of the a-HCN_x films were performed on a multi-technique 100 mm hemispherical electron analyser (CLAM2: VG Microtech), using Al K α radiation (photon energy 1253.6 eV) as the excitation source and the binding energy (BE) of Au (Au 4f_{7/2} : 84.00 eV) as the reference. The XPS spectra were collected in a constant analyser energy mode, at a chamber pressure of 10–8 mbar and pass energy of 23.5 eV at 0.125 eV/step [32]. Fourier transform infrared (FTIR) transmission spectra were obtained by means of FTIR spectrometer Bruker (Vector 22). The plain sample was placed in a vacuum chamber built into the spectrometer in order to minimize the IR signal of water vapour, CO₂ content and noise. The measuring signal passed the optical way with an aperture diameter of 3 mm with spectral resolution 4 cm⁻¹. For optimal signal-to-noise ratio 50 scans were averaged per sample spectrum and apodized by applying of the Norton Beer apodization function for Fourier transformation. Interferograms were zero-filled

using a zero-filling factor of 2. The background spectrum was measured on a pure silicon substrate independently [32]. Elemental analysis was carried out with a CHNS-932 analyzer from LECO using standard conditions. The technique involves combustion of test sample in an oxygen rich environment. The products of combustion in a CHNS analysis (CO₂, H₂O, N₂ and SO₂) are carried through the system by He carrier gas. The combustion products are measured quantitatively by means of a non-dispersive IR absorption detection system, except for the N₂ which is determined via a thermal conductivity detector. Oxygen is measured in a separate VTF furnace. Sample is combusted at high temperature in a carbon rich environment. Resulting CO₂ is measured using the CO₂ IR cell and the percentage of oxygen is determined [32].

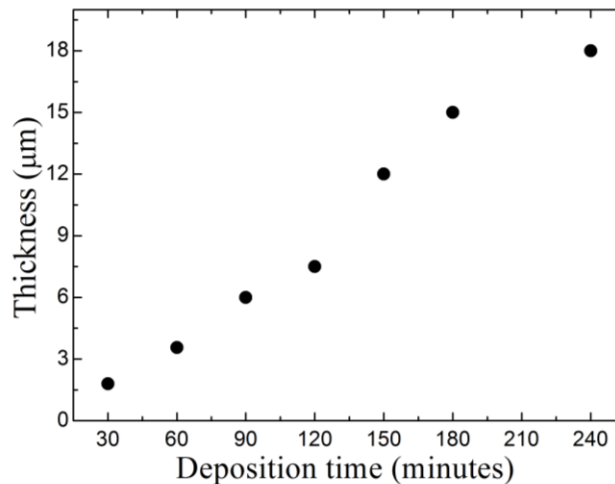


Figure 2. Variation of thickness of the deposited a-HCN_x film as a function of deposition time (minutes).

Thickness of the a-HCN_x film is about 12 μm (deposition time 150 min), measured by Ellipsometer (HORIBA Jobin-Yvon Inc., Edison, USA) in the photon energy range from 1.8 eV up to 4.8 eV at an angle of 70° (due to Brewster's angle of silicon wafer substrate). The complex dielectric function of HCN_x was simulated by the Tauc-Lorentz model oscillator. Finally, the model was fitted to the experimental data using the Levenberg-Marquardt nonlinear least-squares algorithm and in our previous work we have applied this model in hydrogenated carbon nitride (a-H-C_xN_y) film [17, 33]. A few nano meters (~ 4 to 10 nm) layer of Cu was deposited on the surface of the HCN_x film to act as interfacing electrodes. This layer has been introduced to avoid the fluctuation during capacitance measurement. The Cu layer deposition is performed by magnetron deposition unit. The introduction of Cu nano-layer (4 to 10 nm) or Cu clusters in the measurement of low-*k* dielectrics has incrementally improved the surface connectivity during measurement of dielectric constant. It can reduce both resistivity and capacitance between plates. Without Cu layer, we get huge noise signal as well as unstable reading during the dielectric constant measurement. The main reason is the in proper contact to the surface layer. As we move to nano-meter scale the impact of delay is increase enormously [17]. A pallet of a-H-C_xN_y of 10 mm of diameter and 0.42 mm of thickness is prepared by applying force of ten kilo-tonne (Metric ton equals = 10 kN). The P-E loops were taken by applying driving voltage of different time periods (5 mSec, 10 mSec and 20 mSec) [34].

C. Mass spectrum of CH₄/N₂ : Gas composition of stable reaction products only was detected by a mass spectrometer (Balzers QMS 200). It is pumped by a turbomolecular pump (Pfeiffer TSU 062H) to a base pressure of about 10⁻⁸ mbar increasing to about 10⁻⁶ mbar during the experiment. A capillary tube of length 103 cm and inner diameter 0.01 cm connects the mass spectrometer with the plasma chamber. A pressure of 10⁻² mbar at the entrance to the mass spectrometer is maintained during the experiments with the help of a second turbomolecular pump (Balzers 071P). The mass calibration has been done in our previous work in detail [29].

III. RESULTS

Figure 2 shows that the thickness of the deposited a-H-C_xN_y film is increased at longer plasma deposition process. The thickness varies from 1.8 μm to 12 μm as the deposition duration prolonged from 30 to 150 minutes, respectively. Due to transport there is surface contamination and unwanted oxygen adsorb at the surface layer evident from XPS analysis.

A. Chemical property (surface and bulk)

I. X-ray photo electron spectroscopy (XPS)

Figure 3a, shows the full scale (200 eV to 600 eV) spectra of a-H-C_xN_y film. The general strategy of the data evaluation was identical to those for standard spectroscopic techniques. The C-1s peak broadens and also becomes more asymmetric in nature behavior of the surface charge distribution of the silicon substrate covered by the a-H-C_xN_y film. Si (2p) with a Binding Energy (BE) = 99.3 eV was taken as a reference. The calibration details about this chemical shift are discussed in our previous work [32]. A shift of 0.75 ± 0.05 eV was noted which is considered as system calibration for the un-sputtered or virgin films. The film deposited at longer time duration shows higher charging effect (chemical shift towards higher binding energy) compare to the same deposited at 30 mins. The results shown below were corrected by subtracting the experimentally observed shift for all the analyses. A clear image of the possible chemical bonds between nitrogen and carbon can be deduced from the deconvolution of the individual C-1s, N-1s and O-1s lines into Gaussian-shaped lines [32]. This indicates that the carbon is involved in chemical bonds with nitrogen [32].

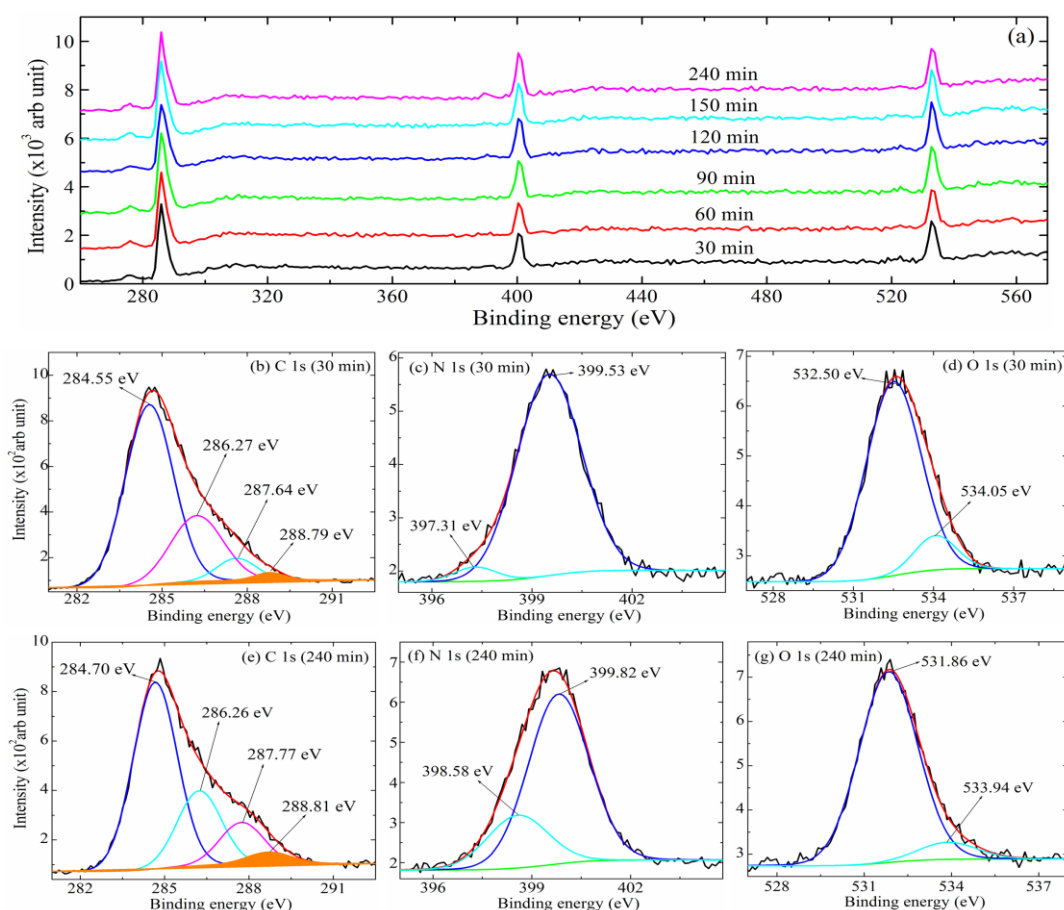


Figure 3. (color online) (a) Full scale (200 eV to 600 eV) XPS spectra of a-HCN_x films. Typical (b) C 1s, (c) N 1s and (d) O 1s are the deconvoluted XPS spectra of a-HCN_x film deposited at 30 min time duration. And similarly, (e) C 1s, (f) N 1s and (g) O 1s are the XPS spectra of the film deposited at 240 mins duration. The XPS spectra were obtained with Al *k*α X-rays at 23.5 eV pass energy at 0.125 eV/step. The data are presented after inelastic background subtraction and using Gaussian fits. The intensity scales for the C, N and O spectra are not the same.

Two categories of films (30 mins and 240 mins) are characterized by XPS and the corresponding deconvoluted spectra are compared according to the binding energy shift and the number of sub-peaks as well. Figure 3 (b, e) shows the XPS C 1s core-level spectra of a-H-C_xN_y films, deposited by 30 min and 240 min time duration, respectively. Figure 3 (b, e), the carbon peak at the binding energy 284.55-284.70 eV is identified as originating from adventitious (extrinsic or accidental) carbon and surface carbon that may have lost its nitrogen neighbours due to reaction with O₂ and CO/CO₂ whenever it is exposed on the air due to transport. Similarly,

the C 1s peak binding energy range at 288.79–288.81 eV is identified as originating from CO type bonds which are depending on the type of bonding such as ketones/aldehydes (–CO/–CHO), carboxyls (–COOH) and carbonates (–CO₃). The presence of the undesired oxygen in the lower nitrogen content films is effectively responsible for the large binding energy shift. From Figure 3 (b, e) we observe that there are two C 1s peaks (2nd and 3rd) in the range of 286.26–to 286.27 eV and 287.64–to 287.77 eV which are assigned as substitutional sp² N in graphite like structures (C=N), threefold coordinated N bonded to fourfold-coordinated sp³ -C≡N, respectively [21, 40-43].

Figure 3 (c, f) shows the XPS N 1s core-level spectra of a-H-C_xN_y films, deposited by 30 min and 240 min time duration, respectively. The N 1s peaks are deconvoluted into three components depending on the nitrogen concentration. There are two nitrogen peaks (1st and 2nd) in the range of 397.31 eV to 398.58 eV and from 399.5 eV to 399.82 eV which are assigned as organic nitriles or isonitriles (R–C≡N or R–NC) and N–O or nitrosomethane-like (R–N=O) species, respectively [39-42]. At higher binding energy the corresponding peak can be assigned to NO, as oxygen was detected as a surface contaminant, and may also result from N₂ molecules trapped in the film [38-43]. Figure 3 (d, g) shows the O1s XPS peak of a-H-C_xN_y film deposited by 30 and 240 mins time duration, respectively. The O1s deconvoluted peaks show two successive peaks in the range at 531.86-532.50 eV and 533.94-534.05 eV assigned as C–O and O–H bond, respectively [38-43].

In the case of N1s, the peak at lower binding energy (397.31 to 398.58 eV) is assigned to nitrogen bonded sp³ carbon and the peak at higher binding energy (399.53 to 399.82 eV) to nitrogen bonded to sp² carbon [38-43]. However, this contradicts the data obtained from pyro-methene which contains N and C atoms, but no sp³ carbon [38-43]. Souto et al. recently compared the valence and core level electronic structures of sputtered a-H-C_xN_y films with a theoretically calculated density of states and core level binding energies of molecules containing sp²/sp³ CN bonds [38]. The combined analysis of core level and valence band spectra lead to the conclusion that the peak at lower energy is related to N atoms in configurations with isolated lone pairs (including threefold-coordinated N atoms bonded to sp³ carbon), while the peak at higher binding energy corresponds to substitution of N in graphite-like configurations, where the lone pairs are involved in stronger bonds (this includes N atoms bonded to sp² C).

II. Fourier transforms infrared spectroscopy (FTIR)

The deposited films required a spectral allowance for an extinction inhomogeneity across the surface and long wave interference effects in the bulk. Therefore base line correction of the recorded spectra was performed by the concave elastic band method. Typical IR transmission spectra are shown in Figure 4, within the range from 4000 cm⁻¹ to 700 cm⁻¹. According with the Bouguer-Lambert-Beer law the interval of integral absorption coefficient $(2.6 \pm 1.5) \times 10^4 \text{ m}^{-1}$ is characteristic for all deposited layers. The transmission spectrum of the deposited hydrogenated carbon-nitride films is characterized by several typical spectral regions [21, 38-43].

The region 3140-3500 cm⁻¹ is attributed as overlapping NH and OH band. More precisely, in the region 3300-3490 cm⁻¹ is referred as anti-symmetric NH₂ stretching band and at 3140 to 3300 cm⁻¹ is H bonded NH symmetric stretching band. However the separation of the overlapped bands is very complicated due to intermolecular interactions as H-bridges, which are very intensive in this region and cause the broadening of the bands. There are two consecutive intervals appeared at 2965 cm⁻¹ and 2884 cm⁻¹ which are attributed to –C–CH₃ and ≡CH band respectively [20, 38-43]. The intensity of the bands is low (absorption up to 1%) and is related with the concentration of methane in the gas discharge. In addition to this, we note (see Fig. 4) a fine absorption band around 1600 cm⁻¹ that is due to the sp² carbon and is normally IR forbidden. The appearance of this feature suggests that the incorporation of nitrogen breaks the sp² symmetry and makes this feature IR active [20, 38-43]. The band from 2250 cm⁻¹ to 2100 cm⁻¹ is triple bond configuration and absorption peak at 2223.83 cm⁻¹ is conjugated stretching vibration band so called nitrile group (–C≡N). The nitrile (–C≡N) peak is shifted from 2223.83 cm⁻¹ to 2182 cm⁻¹ as the deposition time prolonged from 30 mins to 240 mins, respectively. The region from 1580 cm⁻¹ to 800 cm⁻¹ is characterized by a large number of banding vibrations and intermolecular interactions. Absorption in this region can be interpreted as quality of cross-linking of the deposited structure. However, any qualitative properties of the region are not pointed. The broad band including the region at 1600 to 1635 cm⁻¹ usually referred as the band of water molecule deformation vibrations and generally it is weak band. It is obvious that the broad band at 1560 cm⁻¹ to 1680 cm⁻¹ is attributed to amide carbonyl group ((=C=O)NH) and possibly weak C=N stretching band [38-43]. The absorption band observed at 1350 cm⁻¹ -- 1480 cm⁻¹ corresponds to the C–N single stretching bond [45-48].

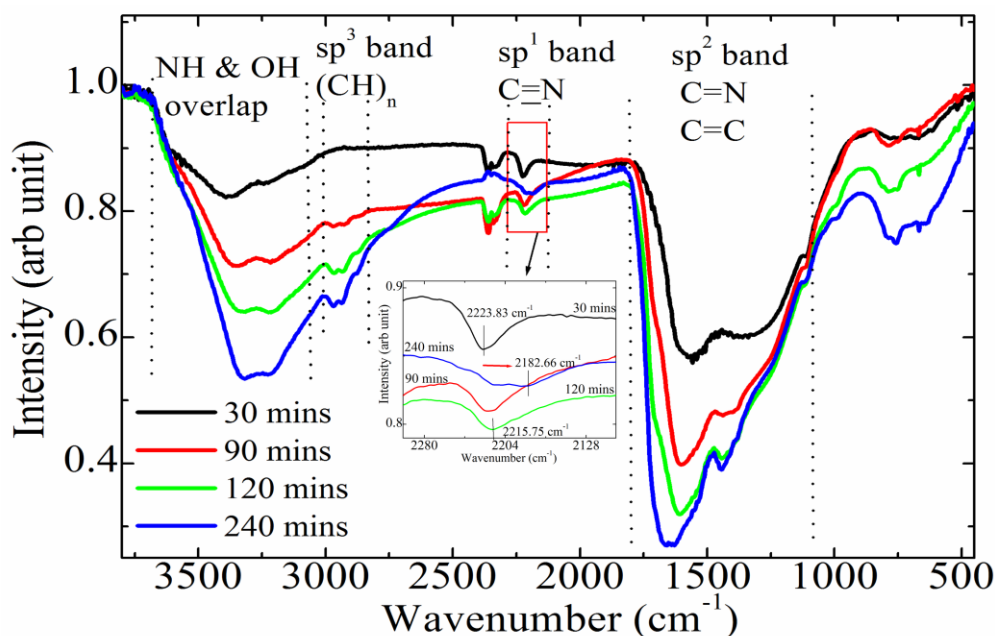


Figure 4. (color online) Full scale FTIR spectra of a-HCN_x film deposited by CH₄/N₂ DBD plasma. The spectra is classified in four different absorption band range as: 3650 cm⁻¹ to 3075 cm⁻¹ for NH/OH region, 3015 cm⁻¹ to 2870 cm⁻¹ for CH₃/CH₂ region, 2270 cm⁻¹ to 2100 cm⁻¹ for sp¹ phase and 1700 cm⁻¹ to 1300 cm⁻¹ for sp² phase.

Finally, the absorption peak at 1080 cm⁻¹ to 1160 cm⁻¹ corresponds to the C-O (ketones group) stretching mode [43-45, 49-51]. The absorption peaks appear in a regular way with different intensities in the IR spectrum. From figure 4, we see that the bands attributed to 1350-1480 cm⁻¹, 1560-1665 cm⁻¹ and 2100-2250 cm⁻¹ respectively, indicating the carbon and nitrogen atoms in the a-H-C_xN_y film are linked as C-N/CH₂ or CH₃, Amide carbonyl group (possibly weak C=N bond) and C≡N bonds [38-43].

III. Elemental analysis

The elemental analysis of the a-H-C_xN_y film removed from the electrodes (Alumina and glass) is (in wt %) C 67.72, H 9.84, N 16.53. After summing up these values (94.09%), it is clear that there is something more in the film, other than C, H, or N. The remaining 5.91 wt% of the sample probably belongs to oxygen. The IR vibrations in the higher frequency region at around 3330 cm⁻¹, assigned partly to C-O-H, and the XPS bands assigned to C=O species as discussed above, are supporting the existence of oxygen in the film, possibly due to absorption of moisture from air by reactive sites of the film. Thus, the final film is made up of the elements C, H, N and O. The fractional empirical formula directly from elemental analysis and calculated by elemental weight of carbon, hydrogen and nitrogen is C_{5.6}H_{9.8}N_{1.2}O_{0.4} [32].

B. Dielectric property of a-H-C_xN_y

We have used the typical charge-voltage characteristic curve (oscilloscopic x-y plot or Lissjous curve) to find out the net charge deposited for a given applied voltage during the plasma deposition. In figure 5, x-and y-axes represent the applied voltage (kV) and the corresponding dissipated charge (C), respectively. The charge is obtained by measuring the voltage across a 10 nF capacitor connected to the ground plate in series. The area under the charge-voltage characteristic curve represents the power dissipated during the CH₄/N₂ plasma barrier discharge [12-17]. The charge - voltage (Q -V loop) characteristic data have been taken for different plasma processing times. We have taken the data every 30 min including starting time. For a longer plasma deposition process the rhomboidal shaped loop gets elongated in y-direction. This indicates that the charge density increases with time on the electrodes area. Due to the applied electric field the ionized gas species or atoms/molecules are driven towards the electrodes surface. The total charge at the electrode surface is given by

$Q (C) = V \times 10 \times 10 \text{ nF}$, where 10 is the probe factor and ground electrode is connected to 10 nF capacitor in series. From definition, polarization is given by the total charge per unit area [32]. Thus we can write,

$$P = \frac{\text{Total charge}}{\text{Electrodes Area}} = \frac{Q_{\max} - Q_{\min}}{\text{Electrodes Area}} \quad (1)$$

The values of Q_{\max} and Q_{\min} are obtained from fig. 5 and in our case area of the electrode is 27.39 cm^2 ($L= 8.3 \text{ cm}$ and $d = 3.3 \text{ cm}$). During the discharge huge amount of charge is accumulated in the electrode area and is retained there as floating charge. The dielectric constant is given by the ratio of the capacitance with medium and the capacitance with vacuum. With the help of fig. 5, we can calculate the capacitances as follows:

$$C_{\text{Vacuum}} = \frac{Q_{\max(v)} - Q_{\min(v)}}{V_{\max(v)} - V_{\min(v)}} \quad \text{and} \quad C_{\text{Plasma}} = \frac{Q_{\max(P)} - Q_{\min(P)}}{V_{\max(P)} - V_{\min(P)}} \quad (2)$$

So, the equivalent dielectric constant of the deposited HCN layer is obtained as,

$$\epsilon_{\text{Equivalent}} = \frac{C_{\text{Plasma}}}{C_{\text{Vacuum}}} \quad (3)$$

Note that the Eq. (2) is true for other DBD systems too. In our DBD system the capacitance in vacuum is $1.0087 \times 10^{-7} \text{ F}$. It has been measured at pressure of 1 mbar.

The *in situ* equivalent dielectric constant of the a-H-C_xN_y layer has been estimated from Eq 3 by using the values of Q_{\max} , Q_{\min} , V_{\max} and V_{\min} from Fig. 5. The capacitance is measured as the charge per unit voltage. It is noticeable that the applied voltage V_{\max} is constant and the quantities Q_{\max} , Q_{\min} , and V_{\min} all vary with time. As a result the charge-voltage characteristic loop gets elongated in y-direction.

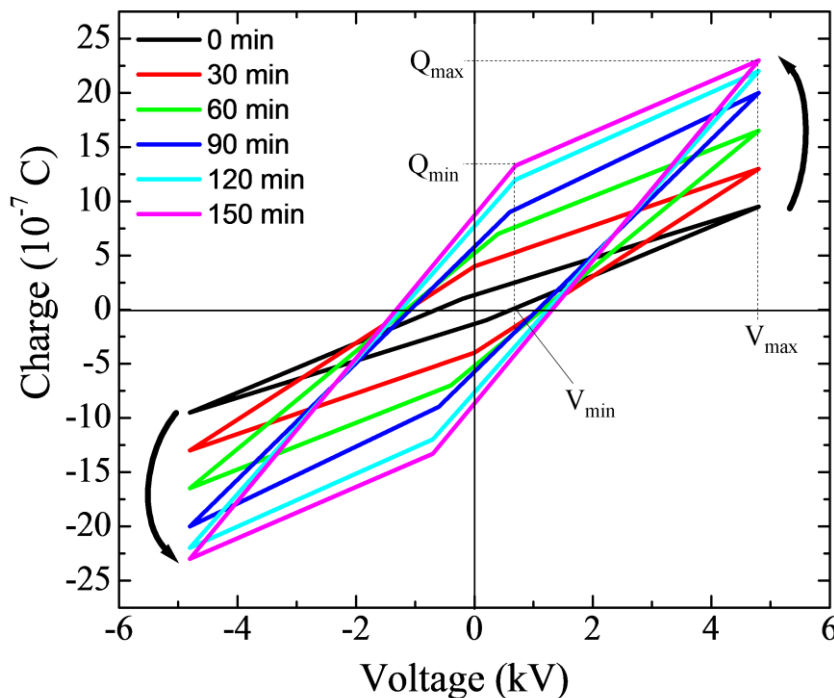


Figure 5. (Color online) Charge - voltage characteristic (Lissajous) curve of CH_4/N_2 DBD plasma for different plasma processing time. The area of the parallelogram is related to the electric power dissipated during the each cycle [12].

Figure 6 (a) shows the variation of polarization with discharge time and it shows that the polarization P varies with time as longer plasma deposition process. In DBD plasma processing the initial electrode temperature decreases with plasma processing time [12]. Figure 6 (b) shows the polarization of bulk a-HCN_x solid as a function of electric field. P-E loop study is providing the qualitative information about the dielectric and resistive property of a-H-C_xN_y at different time scale [33].

Figure 7 (a) shows the variation of (*in situ*) equivalent dielectric constant with time of a-H-C_xN_y layer during the CH₄/N₂ DBD plasma deposition process. The equivalent dielectric constant increases gradually with time but after 90 minutes of deposition it starts to decrease and ultimately attains a saturation value. The approximate error in the dielectric constant measurement is ± 0.1 . Figure 7 (b) shows the variation of (*ex situ*) dielectric constant of a-H-C_xN_y film (measured by impedance analyzer) with the applied frequency. The dielectric constant of a-H-C_xN_y layer decreases from 2.8 to 2.38 as the frequency increases from 1 kHz to 2 MHz. The dielectric constant does not change due to further increase of frequency. The approximate error in the *ex situ* dielectric constant measurement is ± 0.15 .

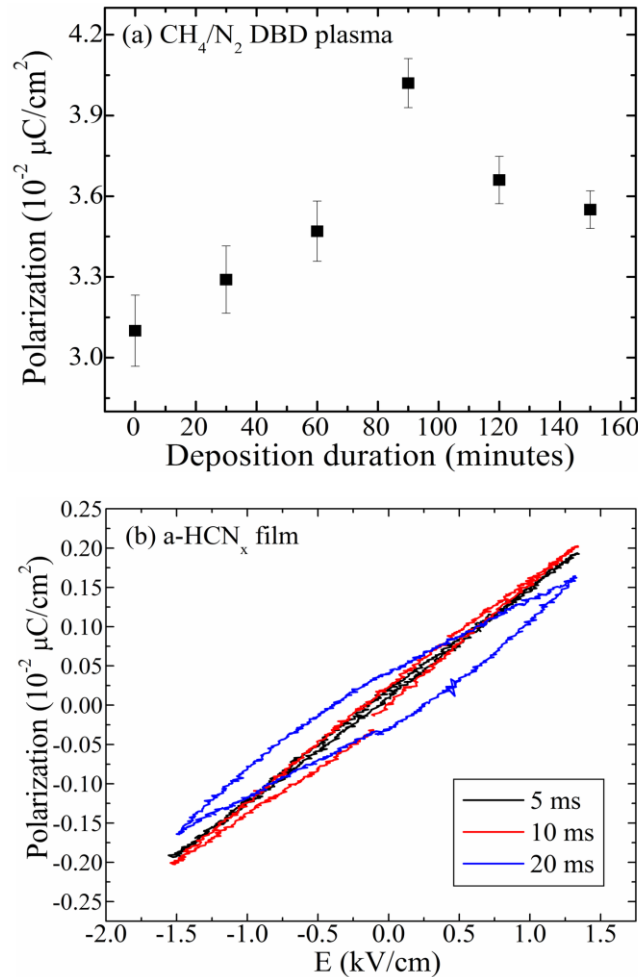


Figure 6. (a) Variations of polarization with deposition time in CH₄/N₂ DBD plasma. The vertical bars represent the error in measurement. (b) Polarization as a Electric field loop of a-HCN_x film at different time period.

C. Surface morphology (SEM)

The island growth (circular spot) on the surface of the deposited amorphous carbon nitride film has been observed in SEM analysis. In our previous study the similar phenomena (bubbles formation) has been observed on amorphous silicon carbide film [17]. Figure 8 (a) and (b) show the SEM image of the film deposited at 30 mins and 240 mins on the Si substrate. The typical SEM image shown in figure was taken from the central region of the deposited film. The morphology developed in the sample is nearly the same all over the sample. The sample is populated with circular carbon rich features of differential sizes. The sample is populated with circular carbon rich features of differential sizes and the sizes (diameters) of these circular spots vary from 250 nm to 800 nm.

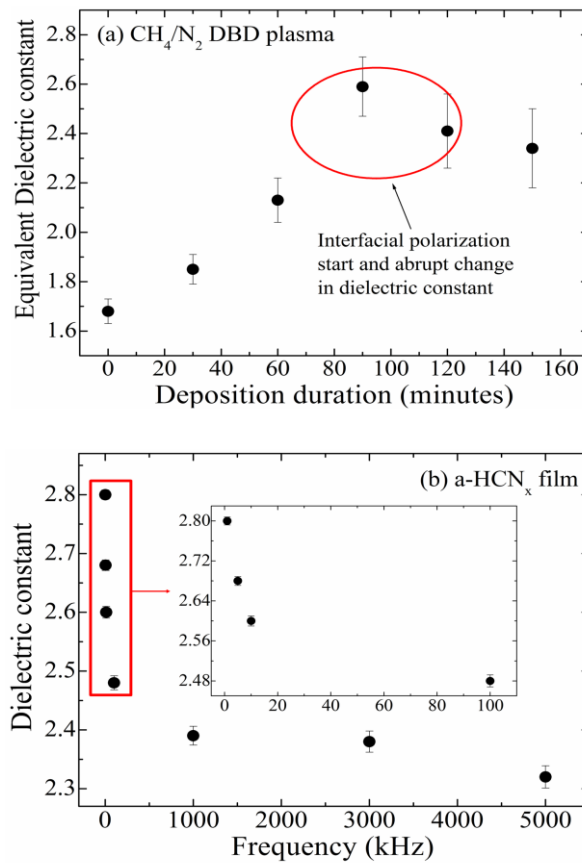


Figure 7. (a) Variations of *in situ* equivalent dielectric constant with respect to the deposition time duration. This curve is plotted with the help of figure 2 and Eqs. (4). (b) Variations of *ex situ* dielectric constant with applied frequency for a-HCN_x film (thickness ~ 20 μm) deposited on *p*-Si (100) wafer (thickness ~ 350 μm). The vertical bars represent the error in measurement.

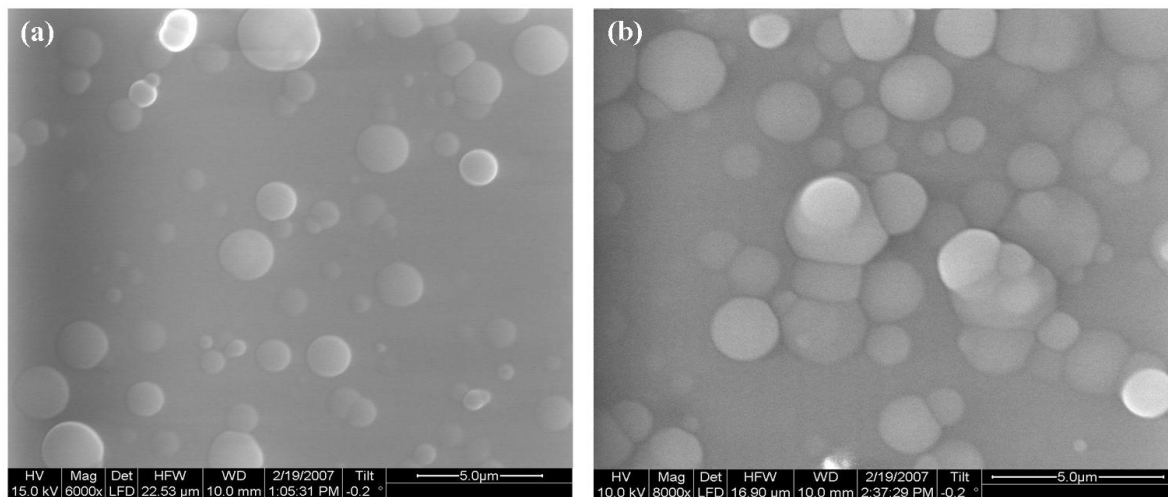


Figure 8. SEM images of hydrogenated carbon nitride film deposited on silicon wafer where a) 30 min deposition time (top view), (b) 240 min deposition time.

D. Mass spectrum analysis

Figure 9a shows two typical mass spectra in the range of mass numbers up to $m/z = 140$ that were obtained after the chamber has been filled with 250 mbar of a CH₄/N₂ gas mixture (mixing ratio 1:2). Figure 9a represents the initial gas composition consisting of nitrogen (N₂) and methane (CH₄) gas (without plasma). Impurities that are

present consist, e.g., of oxygen (O_2) and small amounts of higher hydrocarbons around mass numbers $m/z = 40$, 55, 65, and 78. It should be noted that stable molecules dissociate inside the ion source of the mass spectrometer, giving rise to the formation of unstable radical ions that complicate the data analysis [18, 35, 36]. For example, methane shows up in the mass spectra with masses $m/z = 16$ (CH_4^+), 15 (CH_3^+), 14 (CH_2^+), 13 (CH^+), and even 12 (C^+). Figure 3b displays the mass spectrum obtained from the same gas after the discharge has been operated for 240 min. Several differences are noted in figure 3b, c : (i) a reduction of the methane peaks, (ii) an increase of the hydrogen peak, and (iii) the appearance of higher order hydrocarbon peaks. The experimental results presented below are obtained by subtracting the mass spectra obtained without plasma from those obtained with plasma, e.g. by subtracting the data of black line curve from those of red line curve of figure 3a.

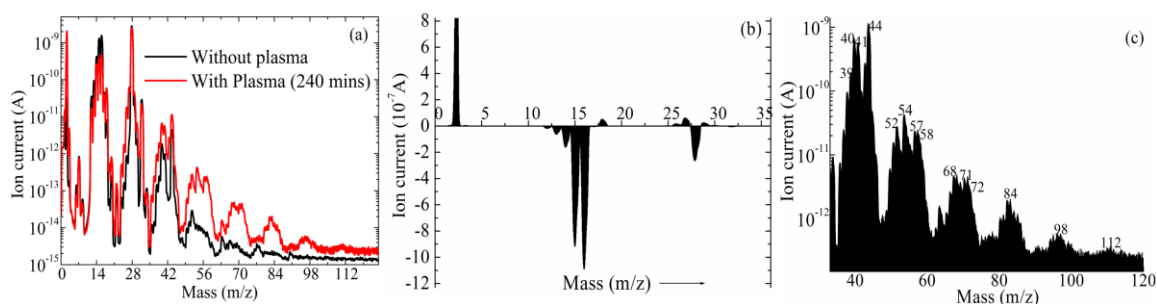


Figure 9. (color online) (a) Mass spectra of with/without plasma (240 mins) obtained by CH_4/N_2 (1:2) gas mixture, (b) difference mass spectrum with and without plasma in the mass range m/z up to 40 for a CH_4/N_2 gas mixture. Note the linear scale. (c) Difference mass spectrum with and without plasma in the mass range m/z 20-140 for a CH_4/N_2 gas mixture [18].

Figure 9b displays the difference spectrum for mass numbers up to $m/z = 40$ on a linear scale obtained by subtracting the data (red and black line curve) of Figure 9a. The production of a large amount of hydrogen (H_2) and a significant consumption of methane is evident. The difference spectrum in the mass range $m/z = 20-140$ is displayed in Figure 9c on a logarithmic scale. Again, the broad prominent peaks, each composed of several individual peaks, are attributed to C_xH_y molecules with x up to 8. In addition, consumption of N_2 is noted which may give rise to the formation of HCN ($m/z = 27$) and its CN ($m/z = 26$) fragment. As the ($m/z = 26$ and 27) peaks overlap with C_2H_2 and C_2H_3 , respectively, no unambiguous identification was possible. The CN can be in form of $C=N$ or $-C\equiv N$ bond.

The time dependency of the hydrogen and methane peaks is shown in our previous study [18]. A pronounced increase of the hydrogen peak, and an approximately exponential decay of the summed methane peaks ($m/z = 12-16$) is noted. Again, a significant amount of the consumed methane is deposited as a yellowish brown film on the electrodes (or on the Si substrate) [29]. Preliminary investigations employing X-ray photoelectron and infrared spectroscopy techniques indicate that the deposited film is composed of carbon and nitrogen (roughly in a ratio of 1:2) and Elemental analysis evident the presence of hydrogen in the deposited film. [32].

IV. DISCUSSION:

From the mass spectrum analysis we can compare the chemical species produced during the deposition process at the same time it can be inferred that the unsaturated charged species flown toward the electrodes surface due to electric field. The gas phase product is not same in the solid phase product since the reaction mechanism is different due to their different thermal equilibrium conditions the discharge processes. In CH_4/N_2 or other hydrocarbon (i.e. $C_2H_4/Ar/N_2$, $C_2H_6/Ar/N_2$ etc) gas mixture plasmas, the gas molecules gain energy from the plasma through inelastic collision and fragmented into energetic smaller molecules [12, 17, 34, 35]. The smaller molecules recombine to form a larger molecule and form oligomer at the surface of the deposited polymer. On the other hand the unsaturated species produced in the gas phase will flow towards the mass spectrometer through the capillary tube due to the pressure gradient. The depositing polymers are constantly irradiated by the plasma until the polymerization process is completed. If the deposited polymers are subject to an interaction of the plasma the polymers may degrade to some extent. During deposition the layer thickness as well as the layer properties such as dielectric constant, polarization of the surface, effective capacitance of the electrode surface, temperature etc change with time [12]. Mass spectrum (fig. 9) shows the production of higher order hydrogenated carbon nitride compound at longer duration of CH_4/N_2 DBD plasma deposition. Higher

order hydrocarbon and associated nitrogen atoms produce the longer molecular chain which may be linear or partly cross-linking or oligomer type.

Gas phase reaction (mass spectrum) shows the production of H₂ gas during the CH₄/N₂ DBD plasma process which is supported by the Elemental analysis of the solid material deposited on the electrodes area during the plasma reaction process. Elemental analysis shows there is 6% H₂ present in the deposited a-HCN_x film. Hydrogenated carbon nitride produced in gas phase (fig 9) is also observed in FTIR and XPS spectrum as C-N associated with hydrogen (fig 3 and 4). Production of C₂H_m species increase the sp² fraction in the film which is supported FTIR spectrum. FTIR shows the elevated NH-OH overlapping region at 3200 cm⁻¹ to 3500 cm⁻¹ region which is due to the production of higher order hydrocarbon.

Figure 4 shows that the Isonitriles absorb bathochromically shifted vs. nitriles due to the slightly lower bond order, in the VB model expressed by a neutral carbene resonance structure with C=N bond (R-N=C: ↔ R-N⁺≡C:). Isonitriles are less stable than nitriles and can rearrange to the latter but are formed primarily in reactions of cationic alkyl species with cyanide anions and may thus be formed under plasma conditions [40-43]. Girard-Lauriault et al. obtained calibration curves from IR spectra of standard materials and showed that the absorption molar absorption coefficients in FTIR of nitriles and isonitriles are very different: isonitriles absorb 14 times more strongly than their nitriles counterparts at equal concentrations [44]. Durrent et al. suggested the possible reaction mechanism of the formation of CN species and that is the detachment of nitrile groups (C:N) from the polymer surface upon cleavage of the carbon bond linking the nitrile terminations to the polymer chains [45]. They mentioned that the plasma induced desorption mechanism would more likely involve nitriles rather than other N-containing functionalities (i.e. amies) because a single C-C bond would have chance to be broken to produce a desorption of the CN bond. Moreover, Seo et al. demonstrated in inductive coupled RF plasma that at a high N₂ gas fraction in the gas mixture for the deposition of a-CN_x films in CH₄/N₂ generated more CN radicals, which resulted not only in more N being incorporated into a-CN_x films but also to a reduction of H passivation that delayed the formation of hybrid bonding between C and N in the films [46]. The influence of H in the a-H-C_xN_y film interrupting the formation of the phase involving C and N bonds since H is preferentially attaches to N. Dilecce et al. observed that CH excitation in the N₂ + CH₄ DBD discharge was not achieved by electron impact on CH but rather by a dissociative excitation of CH₄ [47, 48].

Figure 3 (b-d) shows deconvoluted XPS spectra of C1s, N1s and O1s of a-H-C_xN_y film and the deposition time is 30 minutes. Similarly, figure 3 (e-g) shows the XPS spectra of the same peaks and the deposition time is 240 minutes. In figure 3 (c, f), the N1s peak at lower binding energy (397.31 to 398.58 eV) is assigned to nitrogen bonded sp³ carbon and the peak at higher binding energy (399.53 to 399.82 eV) to nitrogen bonded to sp² carbon [38-42]. The film deposited at 30 mins dominated by N-sp³- bonded carbon whereas 240 mins deposited film shows N-sp²- bonded carbon structure (4c, f). NH₂ and oxide layer is present in both gas and solid phase spectrum (fig 3, 4, 9). Sarra-Bournet et al. mentioned that the plasma polymer case and plasma functionalization of polymers in N₂, N₂-H₂ or NH₃ are similar, where the nitrogen concentration on the surface is lower and the hydrogen concentration in the film is high and that limits the possibility of two or more nitrogen neighbour around the carbon [49, 50]. The XPS measurements and C1 s assignments show that C was bound to N in a mixture of triple-, double-, and single-bonded configurations. The formation of C-C, C=C, and C-H bond in the film is almost similar with deposition time (Fig. 3). In the literature, ageing of amino groups surface densities of nitrogen-containing plasma polymers has been studied [51]. An important component of amines, nitriles, and isonitriles was also observed in FTIR with a smaller intensity of CH_x component (Fig. 4). The spectroscopic analysis suggests that the presence of oxide layer is not the prime cause for binding energy shift. The presence of nitrogen in the solid is also responsible for the higher binding energy shift. The C 1s electron does not take part in chemical bonding during molecule formation, the valence 2s electron has a small probability to be near the most probable vicinity of the 1s electron. The changes of the 2s electron population in the carbon atom will also exert different Coulomb potentials on the 1s electron of the carbon atom. Hence, the binding energy of C 1s is raised. This could be another cause of the chemical shift in higher binding energy. The presence of nitrogen is partly responsible for the binding energy shift for the core level spectrum.

Growth mechanism of the film deposited near atmospheric pressure DBD discharge depends on the various plasma chemical reactions. In atmospheric pressure DBD discharge the electron-induced chemistry is less important as the electron temperatures and degree of ionization are small. Sarra-Bournet et al. mentioned that the desorption of volatile species is quite low under atmospheric pressure and consequently the adsorbed species on the surface dominantly contribute to the coating [50]. This phenomenon should be true for one third of atmospheric pressure (300 mbar) DBD discharge. The purpose of the work at 300 mbar pressure is to avoid uneven short circuit during the discharge process. According to the numerical modelling of the reactive transport in an atmospheric pressure DBD with a longitudinal injection the diffusion of the reactive species is

the limiting factor for the deposition process, whereas gas convection is the dominant force for moving the molecules, it means that radicals associated to the growth must be a boundary layer close to the surface [52].

The thickness of this boundary depends on three things (i) diffusion coefficient of the radicals, (ii) gas flow and (iii) the volume reactivity of the radicals. The diffusion coefficient and gas flow determines the radical's trajectory and volume reactivity determines their lifespan. Radical mean free path is one of the important factors to explain the different reaction zones. The mean free path is around few micrometer ranges in case atmospheric pressure discharges. The radicals arrived at the surface area enable two possible growth mechanism; a homogeneous growth in the gas phase (particle formation) or a heterogeneous growth diffusion-limited aggregation (DLA) on the surface. In DLA method the reactive species approach the surface and adsorb, although they may later move around on the surface, bond permanently or desorb [53]. The structure and its edges increase simultaneously with some fractal structure. The properties of these surfaces and their branching characteristics depend on the growth process as well as on the radical flux, radical energy, sticking probability, mobility of the radical species, substrate temperature etc. The film deposited at atmospheric pressure is predominantly limited by the diffusion that ultimately caused the bubble-like or cauliflower-like coating. Mishra et al. mentioned that the film deposited by in C_2H_2/He or C_2H_4/He DBD plasma shown similar cauliflower-like coating. Figure 8 (a, b) shows the bubble-like coating is developed on the film surface and the circular island growth is increased as the deposition time is increased to 240 mins.

It is observed that at longer CH_4/N_2 DBD plasma deposition process the charge accumulation at the electrodes surface increases with time i.e. the surface polarization increases with time; the equivalent dielectric constant of the DBD system is also found to change nonlinearly with time after the plasma has been switched on. Moreover, a-H- C_xN_y layer when taken outside the DBD chamber is found to have dielectric properties that are different from that found during its deposition process. This is an effect introduced by the reactive nature of the plasma deposition process and the local dielectric relaxation of the deposited molecules. Both the temperature and polarization of the growing films are the results of plasma surface interaction and are expected to be somehow interrelated. Thus it is important to know about the temperature profile of the electrodes surface area during the thin film deposition [12]. So, it is important to know about the *in situ* and *ex situ* dielectric properties of the deposited a-H- C_xN_y layer. This sort of dielectric behavior of hydrogenated carbon nitride film or a- HCN_x solids has not been reported so far [17, 33]. As the frequency of the applied field increases these molecules become unable to follow the rapid alternations of the applied field and as a result the dielectric constant drops. In *ex situ* measurement the dielectric constant of the film at 5 kHz is 2.68 where as its *in situ* measured value at the time when plasma is just switched off is 2.34. Thus the dielectric constant of a-H- C_xN_y film in *ex situ* measurement is greater than that measured during plasma deposition process. The observed difference in *ex situ* and *in situ* values of dielectric constant of a-H- C_xN_y film is probably due to the relaxation of charged masses and molecular species. Relaxation describes the decay of excited states to the ground state after the discharge has been switched off [12]. As a result the orientational polarization of permanent and/or induced electric dipoles increases which in turn increases the dielectric constant of the deposited film. Generally, polarizability increases as volume occupied by electrons increases. It happens due to the larger atoms have more loosely held electrons in contrast to smaller atoms with tightly bound electrons.

The dipole moment is proportional to the size of the separated electrical charges and to the inter-atomic distance between them. The polarizability decreases in the presence of organic groups like $-CH_3$, CH_2 , NH_2 , OH , $C-O$ and increase for $C\equiv N$, $C\equiv C$, $C=C$, $C=O$ etc. Polar polymers have higher dielectric loss since it contain atoms of different electronegativity that give rise to an asymmetric charge distribution. Thus polar polymers have higher dielectric loss and a dielectric constant which depends on the frequency and temperature at which they are evaluated. We have studied the P-E loop (Polarization- Electric field) of a-H- C_xN_y film to get qualitative information of the dielectric and resistive property (fig 7b). A pallet of a-H- C_xN_y of 10 mm of diameter and 0.42 mm of thickness is prepared by applying force of ten kilo-tonne (Metric ton equals = 10 kN). The P-E loops were taken by applying driving voltage of different time periods (5 mSec, 10 mSec and 20 mSec). It was seen that when time period of driving voltage is high the loop is wider and as the time period decreases i.e. frequency increases the loop is narrower and inclined and there is no indication of saturation part for spontaneous polarisation. It shows that a-H- C_xN_y compositions are dielectric with resistive loss. The plots are inclined means sample is dielectric and diminishing of wider loop with the decrease of time period of driving voltage shows its resistive part is compensated with the increase of frequency [34]. The abrupt change in the dielectric constant at a longer deposition time may be due to the interfacial polarization and the local dielectric relaxation of the deposited molecules. The main reason behind this is that at longer deposition time the thickness of the film increases and simultaneously the surface morphology also changes. Amorphous structure and variety of organic chemical bonds largely vary the polarizability of the deposited a-H- C_xN_y film [44]. Hydrogen connected non-volatile compounds always have low polarizability. In our previous study, it is realized that the shake up peak

and fluorescence effect is complementing each other with respect to the presence of organic matrix (Chemfords, NH etc) in the deposited solid. Both shake up peak and fluorescence effect is individually follow the charge transfer model too [39]. Heterogeneous dynamics of the deposited a-H-C_xN_y layer differs from the homogeneous case in the rate at which equilibrium is approached [52]. Constant irradiation of the deposited polymers by the plasma during the polymerization process may also degrade it somewhat [11, 52].

V. CONCLUSION

We proposed a crude assumption to estimate the equivalent dielectric constant of the film during the deposition process. In *ex situ* measurement the equivalent dielectric constant of the film at 5 kHz is 2.68 where as its *in situ* measured value at the time when plasma is just switched off is 2.34. The molecules get thermally relaxed and form either amorphous or periodic arrangement of atom rather than the volatile phase in plasma state. It is probably one of the major cause for the change in dielectric constant. Moreover, gas and surface phase product in CH₄/N₂ DBD plasma are complimenting each other. Mass spectrum of CH₄/N₂ DBD plasma shows the several higher order hydrocarbons (C_xH_y and a-H-C_xN_y, with x is up to 9), different functional CN, NH, CH groups produced in gas phase where as XPS and FTIR spectrum reveals the presence of NH, C=N, C≡N, CH₂, CH₃ and C-N in solid phase. H₂ production increases in gas phase with longer duration of plasma discharge where as it 6% of H₂ obtained by Elemental analysis in solid film. The N/C ratio obtained from the elemental analysis is fitting well with the XPS analysis.

ACKNOWLEDGMENT

Part of this work was supported by the Deutsche Forschungsgemeinschaft (DFG) through Sonderforschungsbereich SFB/TR24 "Fundamentals of Complex Plasmas".

REFERENCE

- [1] H. Kersten, J. Winter, Vacuum **71** (2003) 347.
- [2] G. Morfill, H. Kersten, New J. Phys. **5** (2003) 2003.
- [3] Herrmann, V. Brusler, S. Fiechter, H. Kersten, P. Bogdanoff, J. Electrochemical Society **152** (2005) A2179.
- [4] H. Kersten, H. Steffen, D. Vender, H. E. Wagner, Vacuum **46** (1995) 305.
- [5] T. Farouk, B. Farouk, A. Gutsol and A. Fridman, J. Phys. D: Appl. Phys. **41** (2008) 175202.
- [6] von Keudell and W. Moeller, J. Appl. Phys. **75** (12) (1994) 7718.
- [7] N. Mantzaris, E. Gogolides, A. Boudouvis, A. Rhallabi and G. Turban, J. Appl. Phys. **79** (1996) 3718.
- [8] D. Herrebout, A. Bogaerts, M. Yan and R. Gijbels, J. Appl. Phys. **90** (2001) 570.
- [9] Yu and S. Girschick, J. Appl. Phys. **75** (1994) 3914.
- [10] M. Coltrin and D. Dandy, J. Appl. Phys. **74** (1993) 5803.
- [11] H. Yasuda, J. Macromol. Sci. Chem, A **10** (1976) 383.
- [12] Majumdar, Basudev Ghosh and Rainer Hippler, Phys. Plasmas **17** (2010) 113506.
- [13] R. Hippler, H. Kersten, M. Schmidt, K. H. Schoenbach, Eds., Low Temperature Plasmas, Fundamentals, Technologies, Techniques, Vol. 1 und Vol. 2, Wiley-VCH: Berlin **2008**.
- [14] M. Laroussi, In: Low Temperature Plasmas - Fundamentals, Technologies, Techniques, R. Hippler, H. Kersten, M. Schmidt, K.H. Schoenbach, Eds., Vol. 2, Wiley-VCH: Berlin, **2008**, p. 821-836.
- [15] U. Kogelschatz, Plasma Chem. Plasma Process. **23** (2003) 1.
- [16] H. E. Wagner, R. Brandenburg, K. V. Kozlov, A. Sonnenfeld, P. Michel, J. F. Behnke, Vacuum **71** (2003) 417.
- [17] Majumdar, Sadhan Chandra Das, Thoudinja Shripathi, and Rainer Hippler, Chem. Phys. Lett. **524** (2012) 62.
- [18] Majumdar, J. F. Behnke, R. Hippler, K. Matyash, R. Schneider, J. Phys. Chem. A, **109** (2005) 9371.
- [19] S. P. Lee, Sensors **8** (2008) 1508.
- [20] T. A. Yeh, C.L. Lin, J.M. Sivertsen, J.H. Judy, IEEE Trans. Magn. **27** (1991) 5163.
- [21] G. Fridman, A. D. Brooks, M. Balasubramanian, A. Fridman, A. Gutsol, V. N. Vasilets, H. Ayan and G. Friedman, Plasma Process. Polym. **4** (2007) 370.
- [22] M. Laroussi, I. Alexeff, W. Kang, IEEE Trans. Plasma Sci. **28** (2000) 184.
- [23] Majumdar, R. K. Singh, G. J. Palm, R. Hippler, J. Appl. Phys. **106** (2009) 084701.
- [24] G. Daeschlein, S. Scholz, R. Ahmed, A. Majumdar, T. von Woedtke, H. Haase, M. Niggemeier, E. Kindel, R. Brandenburg, K. Dieter Weltmann, M. Jünger, JDDG. **1007** (2012) 1610.
- [25] P-L Girard-Lauriault, F. Mwale, M. Iordanova, C. Demers, P. Desjardins, M. R. Wertheimer, Plasma Process Polym. **2** (2005) 263.
- [26] F. Mwale, A. Petit, H. T. Wang, P-L Girard-Lauriault, C. J. Hunter, JA Ouellet, M. R. Wertheimer, J. Antoniou. Biomed Eng Online. **6** (2007) 33.
- [27] F. Mwale, P-L Girard-Lauriault, H. T. Wang, S. Lerouge, J. Antoniou, M. R. Wertheimer. Tissue Eng. **12** (2006) 2639.
- [28] Majumdar and R. Hippler, Rev. Sci. Instrum. **78** (2007) 75103.
- [29] Sonnenfeld, T. M. Tun, L. Zajickova, K. V. Kozlov, H.-E. Wagner, J. F. Behnke, R. Hippler, Plasma Poly. **6** (2002) 237.

- [38] H. E. Wagner, R. Brandenburg, K. V. Kozlov, A. Sonnenfeld, P. Michel, J. F. Behnke, *Vacuum* **71** (2003) 417.
- [39] Majumdar, G. Das, K. R. Basvani, J. Heinicke, R. Hippler, *J. Phys. Chem B*, **113** (2009) 15734.
- [40] G. E. Jellison, Jr, V. I. Merkulov, A. A. Poretzky, D. B. Geohegan, G. Eres, D. H. Lowndes, and J. B. Caughman, *Thin Solid Films*, **68** (2000) 377.
- [41] S. C. Das, A. Majumdar, A. Shahee, N. P. Lalla, T. Shripathi, R. Hippler,
- [42] *Ferroelectrics Letters*, **38** (2011) 78.
- [43] L. Boufendi, A. Bouchoule, *Plasma Sources Sci. Technol.* **3** (1994) 262.
- [44] L. Boufendi, J. Hermann, A. Bouchoule, B. Dubreuil, E. Stoffels, W. W. Stoffels,
- [45] M. L. de Giorgi, *J. Appl. Phys.* **76** (1994) 148.
- [46] M. Gioti and S. Logothetidis, *Diamond Relat. Mater.* **12** (2003) 957.
- [47] S. Souto, M. Pickholz, M. C. Santos, F. Alvarez, *Phys. Rev. B* **57** (1998) 2536.
- [48] Majumdar, S. C. Das, T. Shripathi, J. Heinicke, R. Hippler, *Surface Science* **609** (2013) 53.
- [49] J. M. Ripalda, E. Roman, N. Diaz, L. Galan, I. Montero, G. Comelli, A. Baraldi,
- [50] S. Lizzit, A. Goldoni, G. Paolucci, *Phys. Rev. B* **60** (1999) R3705.
- [51] S. Bhattacharyya, C. Cardinaud, G. Turban, *J. Appl. Phys.* **83** (1998) 4491.
- [52] R. Ohta, K. H. Lee, N. Saito, Y. Inoue, H. Sugimura, O. Takai, *Thin Solid Films*
- [53] **434** (2003) 296.
- [54] N. Hellgren, M. P. Johansson, E. Broitman, P. Sandstrom, L. Hultman, J. E. Sundgren, *Thin Solid Films* **382** (2001) 146.
- [55] P-L Girard-Lauriault, P. Desjardins, W. E. S. Unger, A. Lippitz, M. R. Wertheimer, *Plasma Process. Polym.* **5** (2008) 631.
- [56] S. F. Durrant, E. C. Rangel, M. A. B. Demoraes, *J. Vac. Sci Technol. A* **13** (1995) 1901.
- [57] H. Seo, J. H. Kim, K. H. Chung, J. Y. Kim, S. H. Kim, H. Jeon, *J. Appl. Phys.* **98** (2005) 043308-1.
- [58] G. Dilecce, P. F. Ambrico, G. Scarduelli, P. Tosi, S. D. Benedictis, *Plasma Sour. Sci. Technol.* **18** (2009) 015010.
- [59] G. Dilecce, P. F. Ambrico, S. D. Benedictis, Optical diagnostics in dielectric barrier discharges at atmospheric pressure, 19th international symposium of plasma chemistry (ISPC19), Bochum, Germany, (2009).
- [60] Sarra-Bournet, N. Gherardi, H. Glenat, G. Laroche, F. Massines, *Plasma Chem. Plasma Process* **30** (2010) 213.
- [61] Sarra-Bournet, S. Turgeon, D. Mantovani, G. Laroche, *J. Phys. D Appl. Phys.* **39** (2006) 3461.
- [62] F. Truica-Marasescu, P-L. Girard-Lauriault, A. Lippitz, W. E. S. Unger, M. R. Wertheimer, *Thin Solid Films*, **516** (2008) 7406.
- [63] Enache, H. Caquineau, N. Gherardi, T. Paulmier, L. Maechler, F. Massines, *Plasma Process Polym.*, **4** (2007) 806.
- [64] T. A. Witten, L. M. Sander, *Phys Rev B* **27** (1983) 5686.
- [65] K. K. Mishra, R. K. Khardekar, R. Singh, H. C. Pant, *Rev Sci Instrum* **73** (2002) 3251.